

A Novel High Step-Up Converter with a Switched-Coupled-Inductor-Capacitor Structure for Sustainable Energy Systems

Hongchen Liu[†], Jian Ai^{*}, and Fei Li^{**}

^{†,**}Dept. of Electrical Engineering and Automation, Harbin Institute of Technology, Harbin, China

^{*}Dept. of Electrical and Control Engineering, Heilongjiang University of Science and Technology, Harbin, China

Abstract

A novel step-up DC-DC converter with a switched-coupled-inductor-capacitor (SCIC) which successfully integrates three-winding coupled inductors and switched-capacitor techniques is proposed in this paper. The primary side of the coupled inductors for the SCIC is charged by the input source, and the capacitors are charged in parallel and discharged in series by the secondary windings of the coupled inductor to achieve a high step-up voltage gain with an appropriate duty ratio. In addition, the passive lossless clamped circuits recycle the leakage energy and reduce the voltage stress on the main switch effectively, and the reverse-recovery problem of the diodes is alleviated by the leakage inductor. Thus, the efficiency can be improved. The operating principle and steady-state analyses of the converter are discussed in detail. Finally, a prototype circuit at a 50 kHz switching frequency with a 20-V input voltage, a 200-V output voltage, and a 200-W output power is built in the laboratory to verify the performance of the proposed converter.

Key words: Coupled inductor, High step-up voltage gain, Low voltage stress, Switched capacitor

I. INTRODUCTION

In recent years, renewable energy sources have become more and more widely used to replace fossil fuel in many industrial applications. However, such applications include fuel-cell energy-conversion systems and solar-cell energy-conversion systems, where the voltage obtained from the fuel or PV cells is low, so that there is not enough DC voltage to feed the AC utility. In addition, the automobile high-intensity-discharge headlamp operating voltage is much higher than that provided by a battery [1]-[5]. Therefore, it is necessary to step up from a low voltage to a high voltage.

In the conventional converter, a boost converter is used for voltage step-up applications. This is due to the fact that a boost converter can provide a high step-up voltage gain with

an extreme duty cycle in theory. However, in practice, the boost converter voltage gain is usually restricted by the effects of the power switch, rectifier diode, and equivalent series resistance (ESR) of the inductor and capacitor. Moreover, extremely high duty ratio operation will result in serious reverse-recovery problems, low efficiency, high voltage stress of the switch, and electromagnetic interference (EMI) problems [6]-[8]. Thus, a high step-up converter is used for these applications.

Many topologies have been proposed to improve conversion efficiency and to achieve a high step-up voltage gain [7]-[21]. A high step-up voltage gain can be obtained by a switched capacitor technique [7], [8]. Unfortunately, the main switch has a high surge current, the conduction loss is increased, and the cost is increased. Switched inductor technology also extends the voltage gain [7], [9]. Unfortunately, the voltage stresses of the switches of converters are still higher. Therefore, high-voltage rated switches induce serious conduction losses. The voltage-lift technique [10]-[12] developed by Luo can also achieve a high step-up voltage gain. The voltage-lift technique is similar to the Cuk converter, and is based on an energy transfer from

Manuscript received Apr. 7, 2015; accepted Oct. 28, 2015

Recommended for publication by Associate Editor Sangshin Kwak.

[†]Corresponding Author: fenniao@hit.edu.cn

Tel: +88-045186413601, Harbin Institute of Technology

^{*}Dept. of Electrical and Control Engineering, Heilongjiang University of Science and Technology, China

^{**}Dept. of Electrical Engineering and Automation, Harbin Institute of Technology, China

one inductor via an intermediate capacitor to the output. However, the main switch suffers from a high transient current, and the conduction loss is increased.

Converters can achieve a high step-up voltage gain by adjusting the turns ratio of the coupled inductor [13]. Unfortunately, the leakage inductance of the coupled-inductor causes a high voltage spike on the active switches when the switches are turned off [13]-[16]. As a result, converters using a coupled-inductor with an active-clamp circuit and a passive-clamp circuit have been proposed [17]-[21]. Moreover, the leakage energy can be recycled with the help of the clamp circuit.

In this paper, two novel voltage-lift cells are proposed. These cells integrate three-winding coupled inductors technology and switched-capacitor technology, and further extend the voltage gain. At the same time, this paper proposes a novel high step-up voltage gain and a clamp-mode converter which uses a SCIC to achieve a high step-up voltage gain and to reduce the voltage stress of the main switch. The SCIC shares its capacitor with a clamping circuit. Additionally, two capacitors can be charged in parallel and discharged in series via the coupled inductor. However, the leakage inductor of the coupled inductor may cause a high power loss and a voltage spike. Thus, a passive clamping circuit can recycle the leakage-inductor energy of the coupled inductor and clamp the voltage across the main switch. Thus, the reverse-recovery problems in the diodes are alleviated, and the performance of the proposed converter is improved.

II. VOLTAGE-LIFT-TYPE SWITCHED-COUPLED-INDUCTOR-CAPACITOR CELLS

The basic step-up switched-capacitor cells (SC) are constituted with two capacitors and two diodes as shown in Fig. 2. The following are for the discussion about Fig. 1(a), and Fig. 1(b) is similar to Fig. 1(a). When the switching is turned on, D_1 and D_2 turn off, while C_1 and C_2 are discharged in series. When the switching is turned off, D_1 and D_2 turn on, while C_1 and C_2 are charged in parallel.

Converters with switched capacitor (SC) cells can improve the voltage gain when compared to the classic boost converter. Unfortunately, [22] and [23] have a higher components count, their cost is increased, and their output voltages are not continuously adjustable. In recent years, converters with coupled inductors have become more and more widely used in order to solve these problems. These converters can achieve a higher step-up voltage gain by adjusting the turns ratio of the coupled inductor, which can reduce the number of the active switches when compared with converters with SC cells. Unfortunately, the leakage inductance of a coupled-inductor results in a high voltage spike on active switches when the switches are turned off.

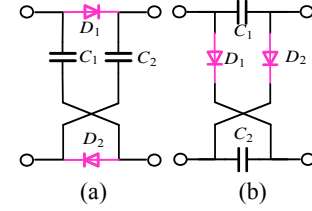


Fig. 1. Step-up basic switching structures. (a) Up I. (b) Up II.

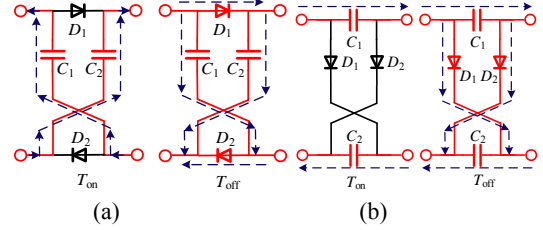


Fig. 2. Switching topologies of the step-up structures. (a) Up I. (b) Up II.

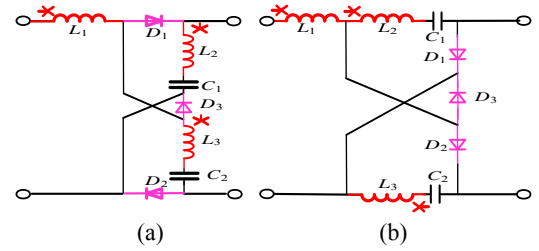


Fig. 3. The proposed basic step-up switching structures. (a) Up I. (b) Up II.

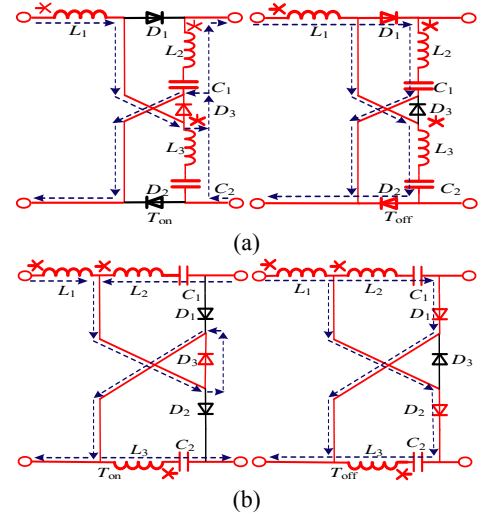


Fig. 4. The current-flow path with the proposed step-up structures. (a) Up I. (b) Up II.

[24] and [25] with coupled inductors can achieve a high step-up voltage gain and the leakage-inductor energy can be recycled to the load. However, in [24] the voltage gain is only equal to 8 and the voltage stress of the output diode is beyond $0.5V_o$ when $n = 2$ and $D = 0.5$. In [25] the voltage gain is only equal to 2 and the voltage stress of the output diode is equal to $0.5V_o$ when $n = 2$ and $D = 0.5$. In order to further

improve the voltage gain, reduce the number of active switches, and reduce the voltage stress of the output diode, the SCICs are proposed in this paper.

The voltage-lift technique is then applied to basic SC cells, which can generate new voltage-lift-type SCIC structures with a higher voltage transfer gain. The basic step-up SCIC structures formed with windings-coupled inductors, diodes and capacitors are shown in Fig. 3. For the convenience of analysis, the switching operations of the proposed SCIC structures are shown in Fig. 4. As shown in Fig. 3(a), the secondary-sides of the windings-coupled inductor are inserted into two branches with the capacitor. The current-flow path is shown in Fig. 4(a). When the switching topologies T_{on} , D_3 turns on, D_1 and D_2 turn off, and L_2 , L_3 , C_1 and C_2 are discharged in series. When the switching topologies are turned off, D_1 and D_2 turn on, D_3 turns off, and the voltage-lift branch (L_2 and C_1) is charged with the voltage-lift branch (L_3 and C_2) in parallel. Fig. 3(b) is similar to Fig. 3(a) in terms of operating principle, and the current-flow path is shown in Fig. 4(b).

III. PROPOSED CONVERTER AND OPERATIONAL PRINCIPLE

Basic step-up switched-capacitor cells (SC) are constituted with two capacitors and two diodes as shown in Fig. 2. The converter with the SCIC led in Fig. 3(b) has not been discussed due to its similarity to Fig. 5(a). The proposed converter with the SCIC Up I is illustrated in Fig. 5(a), which contains an active switch S , three-winding-coupled inductors, three rectifier diodes D_1 , D_2 and D_o , and three capacitors C_1 , C_2 and C_o . It is clear that the leakage inductance of the coupled-inductor will cause a high voltage spike on switch S when the switch is turned off.

In order to suppress the voltage spike by the leakage inductor, clamping circuits composed of diodes D_3 and D_4 and capacitors C_1 and C_2 are shown in Fig. 5(b). Diodes D_3 and D_4 are used to clamp switch S to and prevent the problem of the same time conduction between D_1 and D_o .

The equivalent circuit is shown in Fig. 7. The coupled inductor is modeled as a magnetizing inductor L_m , a primary leakage inductor L_k , and ideal transformers with turns ratios of $N = N_2 : N_1 = N_3 : N_1$ ($N > 1$), where N_1 , N_2 and N_3 are the primary-side turns and the secondary-side turns, respectively. V_{L2} is equal to V_{L3} , and capacitor C_s is the parasitic capacitor of switch S . To simplify the circuit analysis of the proposed converter, the following conditions are assumed. First, all of the components are ideal. The

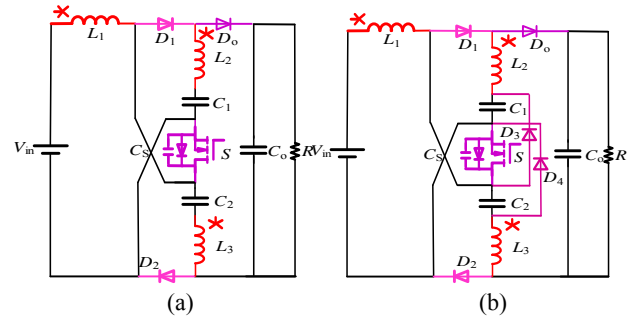


Fig. 5. Circuit configure of the proposed converter.

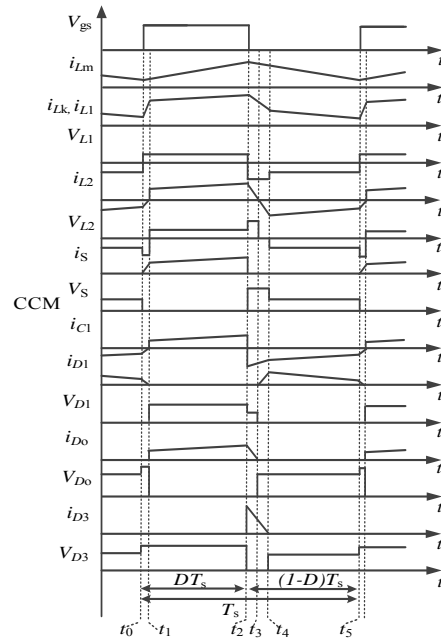


Fig. 6. Some typical waveforms of proposed converter at CCM operation.

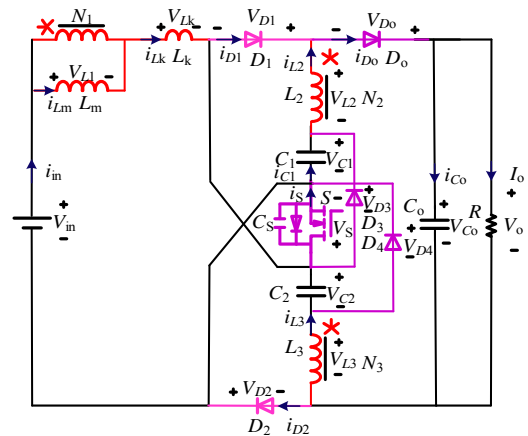


Fig. 7. Equivalent circuit model of the proposed converter.

ON-state resistance R_{DS} of the active switches, the forward voltage drop of the diodes and the ESR of the coupled inductor and all of the capacitors are ignored. Second, capacitors C_o , C_1 and C_2 are sufficiently large, the voltages V_{C1} and V_{C2} are equal to V_{CC} , and the voltages across the

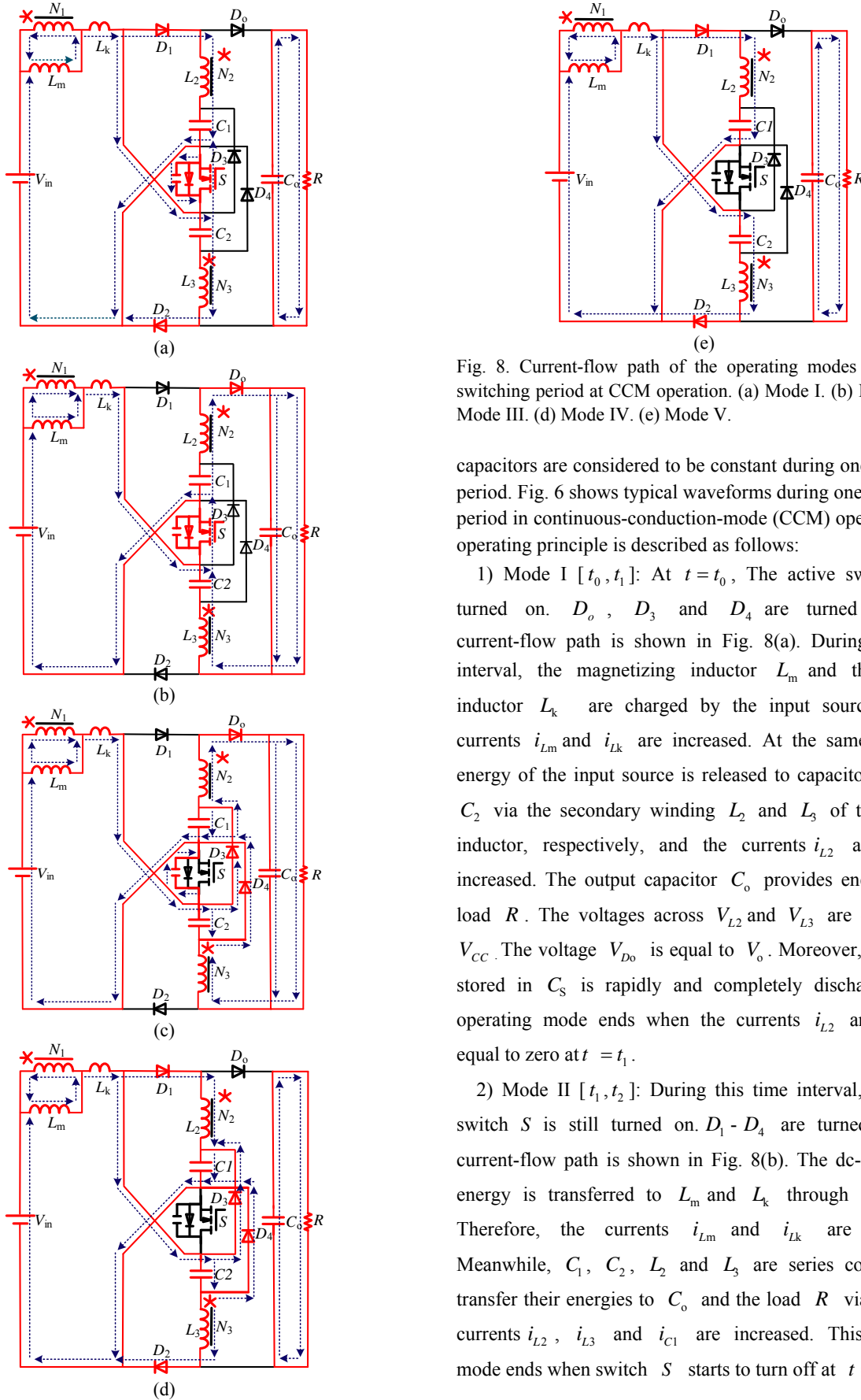


Fig. 8. Current-flow path of the operating modes during one switching period at CCM operation. (a) Mode I. (b) Mode II. (c) Mode III. (d) Mode IV. (e) Mode V.

capacitors are considered to be constant during one switching period. Fig. 6 shows typical waveforms during one switching period in continuous-conduction-mode (CCM) operation. The operating principle is described as follows:

1) Mode I [t_0, t_1]: At $t = t_0$, The active switch S is turned on. D_o , D_3 and D_4 are turned off. The current-flow path is shown in Fig. 8(a). During this time interval, the magnetizing inductor L_m and the leakage inductor L_k are charged by the input source and the currents i_{Lm} and i_{Lk} are increased. At the same time, the energy of the input source is released to capacitors C_1 and C_2 via the secondary winding L_2 and L_3 of the coupled inductor, respectively, and the currents i_{L2} and i_{L3} are increased. The output capacitor C_o provides energy to the load R . The voltages across V_{L2} and V_{L3} are clamped at V_{CC} . The voltage V_{D_o} is equal to V_o . Moreover, the energy stored in C_s is rapidly and completely discharged. This operating mode ends when the currents i_{L2} and i_{L3} are equal to zero at $t = t_1$.

2) Mode II [t_1, t_2]: During this time interval, the active switch S is still turned on. $D_1 - D_4$ are turned off. The current-flow path is shown in Fig. 8(b). The dc-source V_{in} energy is transferred to L_m and L_k through switch S . Therefore, the currents i_{Lm} and i_{Lk} are increased. Meanwhile, C_1 , C_2 , L_2 and L_3 are series connected to transfer their energies to C_o and the load R via D_o . The currents i_{L2} , i_{L3} and i_{C1} are increased. This operating mode ends when switch S starts to turn off at $t = t_2$.

3) Mode III $[t_2, t_3]$: At $t = t_2$, switch S is turned off. The current-flow path is shown in Fig. 8(c). During this mode, the voltage across switch S increases rapidly. The voltages across L_2 and L_3 are clamped at $(V_o - V_{cc})/2$, and the voltage across the active switch S is clamped at V_{cc} , because the clamping diodes D_3 and D_4 are turned on. The voltages across D_1 and D_2 are clamped at V_{L2} and V_{L3} , respectively. As a result, they are reverse-biased. The energies of inductors L_2 and L_3 with capacitors C_1 and C_2 are released to the output capacitor C_o and the load R . The voltage V_{L1} is equal to $V_{in} - V_{cc}$. This operating mode ends when the current i_{L2} becomes zero at $t = t_3$.

4) Mode IV $[t_3, t_4]$: At $t = t_3$, the output diode is turned off, and the rectifier diodes D_1 and D_2 are turned on. The current-flow path is shown in Fig. 8(d). The voltage across L_1 is still equal to $V_{in} - V_{cc}$, and the voltages across L_2 and L_3 are clamped at $-V_{cc}$. However, the voltage across switch S is clamped at V_{cc} . The primary side of the coupled inductor is in series with the input source and the secondary side L_2 of the coupled inductor to release their energies to the capacitor C_1 via the diode D_1 . At the same time, the primary side of the coupled inductor is in series with the input source and the secondary side L_3 to release their energies to the capacitor C_2 via the diode D_2 , and the currents i_{Lk} , i_{Lm} and i_{L2} are reduced. Thus, the clamping diodes D_3 and D_4 are cut off at $t = t_4$, and this operating mode ends.

5) Mode V $[t_4, t_5]$: During this time interval, switch S is still turned off. The clamping diodes D_3 and D_4 are turned off, and the current-flow path is shown in Fig. 8(e). The primary side of the coupled inductor, the secondary side winding L_2 and the input source are in series to transfer their energies to the capacitors C_1 via the rectifier diode D_1 . Meanwhile, the capacitor C_2 is charged by the input source, the primary side of the coupled inductor and the secondary side winding L_3 via the rectifier diode D_2 . This mode ends at $t = t_5$ when switch S is turned on at the beginning of the next switching period.

IV. STEADY-STATE ANALYSIS

A. CCM Operation

In CCM operation, the time durations of modes I, III and IV are very short when compared to one switching period.

Thus, only modes II and V are considered. In order to analyze the voltage gain of the proposed converter, the voltages across the capacitors C_1 and C_2 are assumed to be:

$$V_{C1} = V_{C2} = V_{CC} \quad (1)$$

The coupled-coefficient k and the turns ratio n of the coupled-inductor are assumed to be:

$$n = N_2 / N_1 = N_3 / N_1 \quad (2)$$

$$k = L_m / (L_m + L_k) \quad (3)$$

During mode II, the following equations can be written based on Fig. 8(b):

$$V_{L1}^{II} = kV_{in} \quad (4)$$

$$2nkV_{L1}^{II} = V_o - 2V_{CC} \quad (5)$$

Substituting (4) into (5), the voltages of the capacitors C_1 and C_2 are obtained as:

$$V_{C1} = V_{C2} = V_{CC} = (V_o - 2nkV_{in}) / 2 \quad (6)$$

During mode V, the following equations can be formulated based on Fig. 8(e):

$$V_{in} + V_{L1}^V + nV_{L1}^V = V_{CC} \quad (7)$$

Where the voltage V_{L1}^V is found to be:

$$V_{L1}^V = (V_{in} - V_{CC}) / (n + 1) \quad (8)$$

Using the volt-second balance principle on L_1 yields:

$$\int_0^{DT_s} V_{L1}^{II} dt + \int_{DT_s}^{T_s} V_{L1}^V dt = 0 \quad (9)$$

Substituting (4) and (8) into (9), the voltages across the capacitors C_1 and C_2 and the voltage gain are obtained as:

$$V_{C1} = V_{C2} = V_{CC} = (1 + Dk^2 + nDk^2 - D)V_{in} / (1 - D) \quad (10)$$

$$M_{CCM} = 2(nDk^2 + Dk^2 + nk + 1 - nDk - D) / (1 - D) \quad (11)$$

It can be seen that the voltage gain is influenced by the turns ratio and the leakage coefficient. The relationships between the voltage gain, the duty ratio and the coupling coefficients of the coupled inductor are shown in Fig. 9. It can be seen that the voltage gain is less sensitive to the coupling coefficient. Thus, if the impact of the leakage inductances of the coupled inductor is neglected, the coupled coefficient k is equal to 1. The ideal voltage gain can be simplified as:

$$M_{CCM} = V_o / V_{in} = 2(n + 1) / (1 - D) \quad (12)$$

The voltage gain of a traditional boost converter is $1/(1-D)$. In [7], the basic switch-capacitor boost voltage gain is $1 + D/(1-D)$. The voltage gain in [20] is $(1 + nD)/(1-D)$ and the voltage gain in [21] is $(1 + 2n - nD)/(1-D)$. They have a lower voltage gain when compared with the proposed converter.

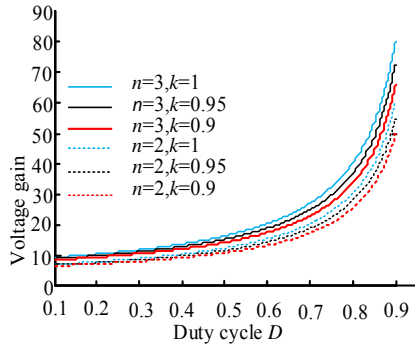


Fig. 9. Voltage gain versus duty ratio at CCM operation under $n = 2$ and various k .

B. Boundary Operating Condition

Since the time durations $[t_0, t_1]$ and $[t_2, t_4]$ are very short when compared to one switching period, these two time durations are not considered. When the proposed converter is operated in the boundary conduction mode, the peak value of the secondary side current of the coupled inductor is given as:

$$I_{L2p} = nkDT_s V_{in} / L_2 \quad (13)$$

Thus, the peak current of the output diode is given as:

$$I_{Dop} = nkDT_s V_{in} / L_2 \quad (14)$$

At the steady state, the average value of i_{Do} is equal to I_o . Thus:

$$I_{Dop} = nkDT_s V_{in} / L_2 = I_o = V_o / R \quad (15)$$

Then, the time constant τ_{L2} of the secondary side for the coupled inductor is derived as:

$$\tau_{L2} \equiv L_2 / RT_s = L_2 f_s / R \quad (16)$$

Where f_s is the switching frequency.

Substituting (11) and (16) into (15), the boundary time constant τ_{L2B} for the secondary side of the coupled inductor can be given as:

$$\tau_{L2B} = nD(1-D) / 2(n+1) \quad (17)$$

If τ_{L2} is larger than τ_{L2B} , the proposed converter is operated in the CCM. The curved line of τ_{L2B} is shown in Fig. 10.

C. Voltage and Current Stresses on Power Devices

According to the operating principle, the voltage and current stresses on power devices are discussed as follows. If the impact of the leakage inductor of the coupled inductor is ignored, the voltage stresses on switch S , $D_1 - D_3$ and D_o are given as:

$$V_{DS} = V_{CC} = (1+nD)V_{in} / (1-D) = (nD+1)V_o / 2(n+1) \quad (18)$$

$$V_{D1} = V_{D2} = (1+n)V_{in} / (1-D) = V_o / 2 \quad (19)$$

$$V_{D3} = V_{D4} = V_{CC} = \frac{1+nD}{1-D} V_{in} = \frac{nD+1}{2(n+1)} V_o \quad (20)$$

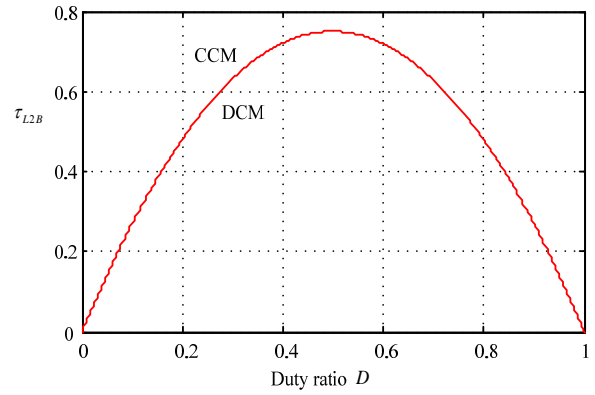


Fig. 10. Boundary condition of the proposed converter with $n=2$ and $k=1$.

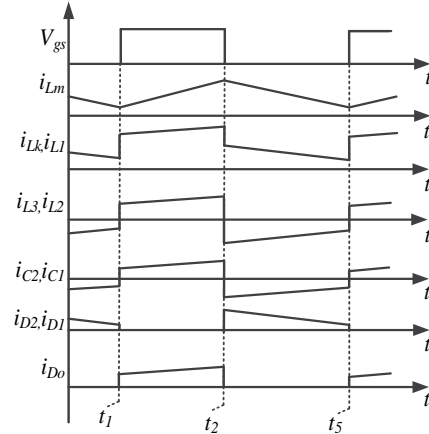


Fig. 11. Simplified waveforms.

$$V_{Do} = V_o \quad (21)$$

From (14) and (15) the current stresses that flow through D_1 , D_2 and D_o are found to be:

$$I_{D1} = I_{D2} = I_{Do} = I_o + I_{Dop} / 2 = V_o / R + nkDT_s V_{in} / L_2 \quad (22)$$

In order to simplify the current calculation, the extremely short time intervals $[t_0 - t_1]$, $[t_2 - t_3]$ and $[t_3 - t_4]$ are ignored. The magnetizing current is considered to be a constant since the magnetizing inductor L_M is large enough. The simplified waveforms of the proposed converter are shown in Fig. 11.

According to the current balance law, the on-state average current of capacitor C_1 can be expressed as:

$$I_{C1(on)} = I_o / D \quad (23)$$

According to the current balance law, the off-state average currents of capacitor C_1 and diodes D_1 and D_2 can be represented as:

$$I_{D1(off)} = I_{D2(off)} = I_{C1(off)} = I_o / (1-D) \quad (24)$$

Thus, based on Fig.11 and equation (24), the magnetic average current of the coupled inductor can be represented as:

$$I_{LM} = 2(N+1)I_o / (1-D) \quad (25)$$

TABLE I
PERFORMANCE COMPARISONS AMONG DIFFERENT CONVERTERS

Topology	Converter in [26]	Converter in [27]	Converter in [28]	Converter in [29]	Converter in [30]	Proposed converter
Numbers of Active switches	1	2	1	2	2	1
Numbers of diodes	5	3	3	6	2	5
Voltage gain	$\frac{2+n}{2-2D}$	$\frac{1+nD}{1-D}$	$\frac{2+nD}{1-D}$	$\frac{1+2nD+D}{1-D}$	$\frac{1+nD}{1-D}$	$\frac{2n+2}{1-D}$
Voltage stress of active switches	$\frac{2V_o}{2+n}$	$\frac{V_o}{1+nD}$	$\frac{V_o}{2+nD}$	$\frac{V_o+V_oND}{1+D+D2N}$	$\frac{V_o}{1+n}$	$\frac{(nD+1)V_o}{2(n+1)}$
Voltage stress of output diodes	$\frac{2V_o}{2+n}$	$\frac{V_o}{1+nD}$	$\frac{(n+1)V_o}{2+nD}$	$\frac{V_o+V_oND}{1+D+D2N}$	V_o	$\frac{V_o}{1+nD}$

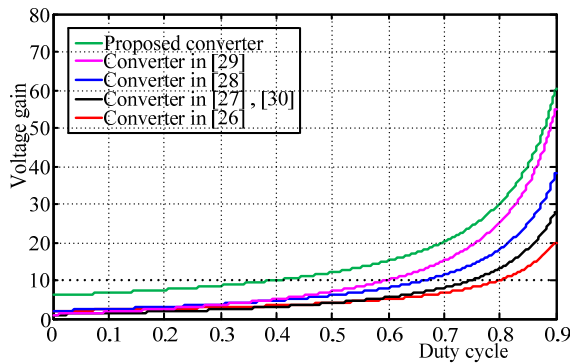


Fig. 12. Voltage gain comparison.

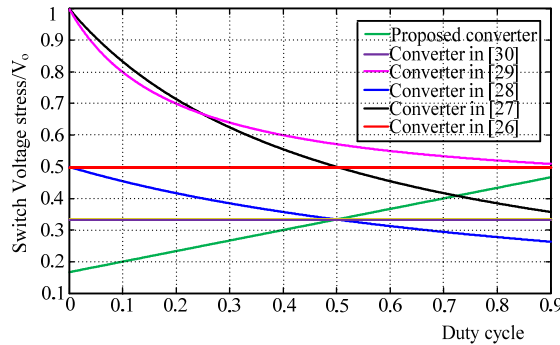


Fig. 13. Active switch voltage stress comparison.

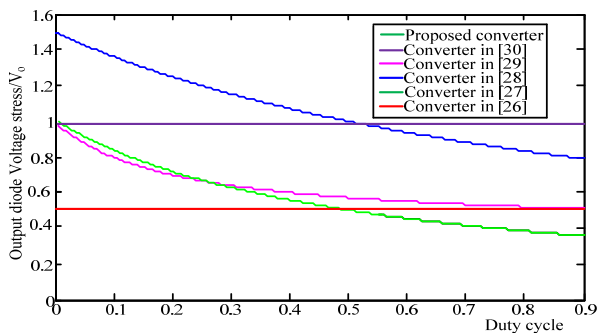


Fig. 14. Output diode voltage stress comparison.

D. Performance Comparison

To further demonstrate the performance of the proposed converter, table I shows a comparison of the performances between the voltage-clamped DC–DC converter in [26], the coupling inductor boost converter in [27], the coupled inductor voltage-lift converter in [28], the coupled inductor active-network converter in [29], the coupled inductor voltage doubler cell converter in [30], and the proposed converter.

The voltage gain of the proposed converter is compared with that of the step-up converters in Fig. 12 when $N = 2$ and $K = 1$. It is observed that the voltage gain of the proposed converter is higher than that of the others.

The relationship between the voltage stress of the active switch and variable duty cycle is described in Fig. 13 when $N = 2$. The active switch stress of the proposed converter is lower to under $D < 0.5$.

The relationship between the voltage stress of the output diode with a variable duty cycle is shown in Fig. 14 when the turns ratio is equal to 2. When the duty cycle is more than about 0.5, the output diode voltage stress of the proposed converter is lower.

Compared to the voltage-clamped DC–DC converter in [26], with the same component count, the voltage gain of the proposed converter has an advantage, and the output diode voltage stress of the proposed converter is lower when the duty cycle is beyond 0.5. When the duty cycle is less than 0.5, the output diode voltage stress of the converter in [26] is lower. Fortunately, the proposed converter has an obviously advantage in terms of the active switch voltage stress. Therefore, low R_{DS} MOSFETs can be used. This is beneficial for improving the converter efficiency.

Comparing the coupling inductor boost converter in [27], the diode count of the presented converter is greater.

TABLE II

SYSTEM SPECIFICATIONS OF THE PROPOSED CONVERTER

System parameters	Specifications
Input voltage V_{in}	20V
Output voltage V_o	200V
Rated power P_o	200W
Switching frequency f_s	50kHz

TABLE III

SYSTEM SPECIFICATIONS OF THE PROPOSED CONVERTER

Components	Specifications
MOSFET Switch S	SiHG73N60E
Diodes $D_o - D_4$	IDH12S60C
Output capacitor C_o	470 μ F, 0.1 μ F
Capacitors C_1, C_2	10 μ F, 0.1 μ F
Coupling inductors	Core-NPS306060, $N = N_2 / N_1 = N_3 / N_1$, $L_p = 137.6\mu$ H, $L_s = 548.5\mu$ H

However, the active switch count is lower and the voltage gain of the presented converter has an advantage. The output diode voltage stress is equal to the presented converter. When the duty cycle is beyond about 0.72 the active switch voltage stress of the presented converter is more than the converter in [27]. When the duty cycle is lower than 0.72 the active switch voltage stress has an advantage especially when the duty cycle is lower than 0.5. In this paper, the duty cycle is about 0.4. Therefore, low R_{DS} MOSFETs can be used.

Compared to the coupled inductor voltage-lift converter in [28], the proposed converter has more diodes. Fortunately, the voltage gain and the output diode voltage stress of the presented converter have advantages. When the duty cycle is more than about 0.5, the active switch voltage stress has no advantage. However, the active switch voltage stress is lower

when the duty cycle is less than 0.5. In this paper, the duty cycle is about 0.4. Therefore, low R_{DS} MOSFETs can be used.

Compared to the coupled inductor active-network converter in [29], the voltage gain and active switch voltage stress of the proposed converter have advantages. In addition, the output diode voltage stress of the proposed converter is lower when the duty cycle is beyond about 0.27, and the proposed converter has fewer diodes and switches.

Compared to the coupled inductor voltage doubler cell converter in [30], the voltage gain and output diode voltage stress of the proposed converter have advantages. The active switch voltage stress is low when $D < 0.5$, and the active switch count of the proposed converter is lower.

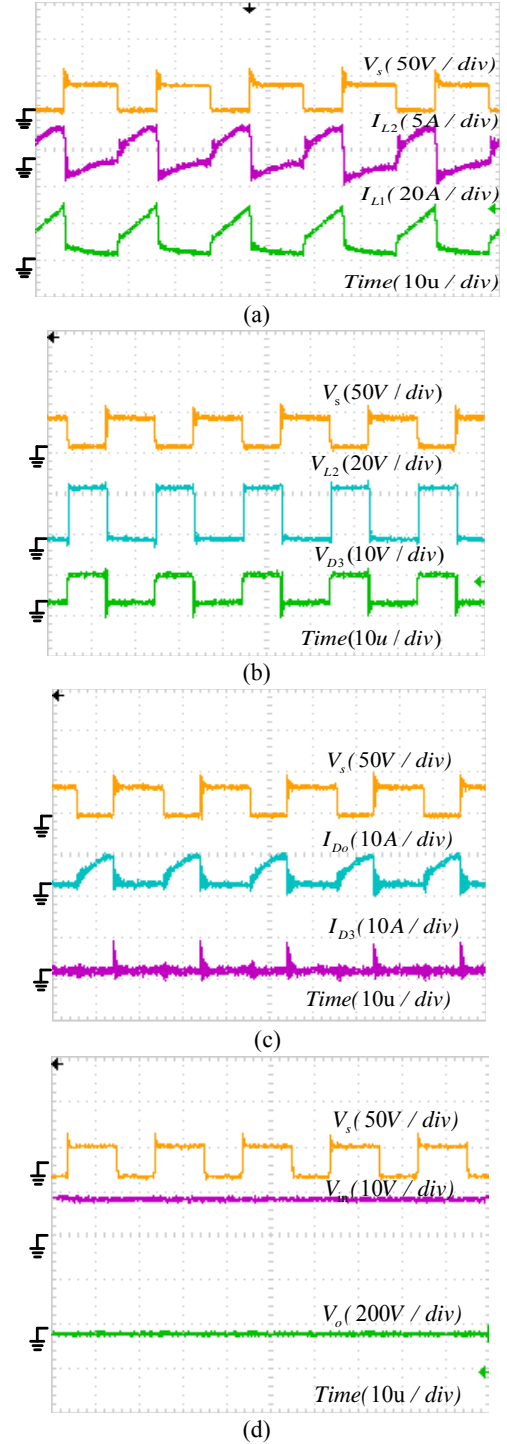


Fig. 15. Experimental waveforms of proposed converter under full-load 200W.

V. EXPERIMENTAL RESULTS

To verify the performance of the proposed converter, a prototype circuit is implemented in the laboratory. Table II shows the system specifications of the proposed converter, and Table III shows the component specifications used in the proposed converter. The specifications are as follows:

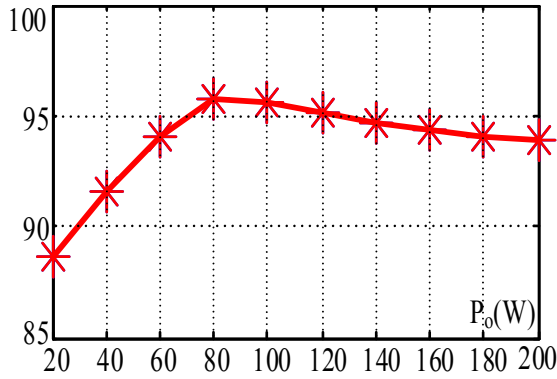


Fig. 16. Experimental conversion efficiency

A. The magnetizing inductance design

The magnetizing inductor can be designed by setting an acceptable current ripple on the magnetizing inductor, which is given by:

$$L_M \geq V_{in} D / K_{L_M} I_{L_M} f_s \quad (26)$$

By combining (25) and (26), and collecting the terms, the magnetizing inductance can be computed as:

$$L_M \geq V_{in} D(1-D) / 2K_{L_M} I_o (N+1) f_s \quad (27)$$

Where K_{L_M} is the current ripple coefficient.

Based the relative equation in section V, the numerical design of the magnetizing inductance of the coupled inductor, the output capacitor and the clamped capacitors are shown as:

$$L_M \geq V_{in} D(1-D) / 2K_{L_M} I_o (N+1) f_s \approx 80.6 \mu\text{H} \quad (28)$$

B. Turns ratio design

Since the turns ratio of the coupled inductor determines the voltage stress of the switch and the operational duty-cycle of the converter, it is the key parameter in the circuit design. The turns ratio can be obtained when the duty-cycle is constant, which is given by:

$$N = (V_o(1-D) - 2V_{in}) / 2V_{in} \quad (29)$$

Some of the key figures are given as Fig. 15 under a full-load. Fig. 15 shows the measured waveforms for a full-load. The proposed converter is operated in the CCM. The waveforms demonstrate that the steady-state analysis is correct. In the measured waveforms, the duty cycle is 41% and the voltage stress on switch S is equal to 35V during the switch off and it is shortly clamped at 54V. Therefore, a low-voltage-stress switch is adopted to achieve high efficiency for the proposed converter. Fig. 15(a) shows the switch voltage V_s , the coupled inductor currents i_{L1} and i_{L2} . The waveforms agree with the theoretical analysis. Fig. 15(b) shows the switch voltage V_s , the coupled inductor voltage V_{L1} , and the clamped diode reverse-biased voltage V_{D3} . Fig. 15(c) shows the switch voltage V_s , the clamped diode

current i_{D3} , and the output diode current i_{D0} . Fig. 15(d) shows that the output voltage V_s is equal to 197V.

Fig. 16 shows the conversion efficiency of the proposed converter, where the maximum efficiency is around 95.8% at $P_o = 80$ W, and the full-load efficiency is approximately 93.7% under 200W with a 20V input voltage.

VI. CONCLUSION

In this paper, a novel switched-coupled-inductor-capacitor topology with a high voltage ratio is proposed and the steady state analysis is given. A passive lossless clamping circuit is introduced to suppress voltage spikes across the switch. Compared to traditional high step-up DC-DC converters, it has following main advantages:

- (1) A high voltage gain can be achieved with a reduced magnetic size.
- (2) A single active switch is required, implying a very simple control circuit. The inrush current problem of the switched-capacitor circuit is well restrained by the leakage inductance of the coupled inductor.
- (3) A low voltage stress power switch can be selected, which can help reduce both the on-state resistance of the switch and the loss.

ACKNOWLEDGMENT

This work is supported by the National Natural Science Foundation of China (no. 51107016), specialized research fund for the doctoral program of higher education (20132302110013) and the Postdoctoral science-research developmental foundation of Heilongjiang province (no. LHB-Q12086).

REFERENCES

- [1] L. Palma, M. H. Todorovic, and P. Enjeti, "A high gain transformerless DC-DC converter for fuel-cell applications," in *IEEE 36th Power Electronics Specialists Conference*, pp. 2514–2520, Jun. 2005.
- [2] S. V. Araujo, R. P. Torrico-Bascope, and G. V. Torrico-Bascope, "Highly efficient high step-up converter for fuel-cell power processing based on three-state commutation cell," *IEEE Trans. Ind. Electron.*, Vol. 57, No. 6, pp. 1987–1997, Jun. 2010.
- [3] V. V. R. Scarpa, S. Buso, and G. Spiazzi, "Low-complexity MPPT technique exploiting the PV Module MPP locus characterization," *IEEE Trans. Ind. Electron.*, Vol. 56, No. 5, pp. 1531–1538, May 2009.
- [4] B. Yang, W. Li, Y. Zhao, and X. He, "Design and analysis of a grid connected PV power system," *IEEE Trans. Power Electron.*, Vol. 25, No. 4, pp. 992–1000, Apr. 2010.
- [5] M. Yilmaz and P. T. Krein, "Review of the impact of vehicle-to-grid technologies on distribution systems and

- utility interfaces," *IEEE Trans. Power Electron.*, Vol. 28, No. 12, pp. 5673–5689, Dec. 2013.
- [6] X. Hu and C. Gong, "A high voltage gain DC-DC converter integrating coupled-inductor and diode-capacitor techniques," *IEEE Trans. Power Electron.*, Vol. 29, No. 2, pp. 789–800, Feb. 2014.
 - [7] B. Axelrod, Y. Berkovich, and A. Ioinovici, "Switched-capacitor/switched-inductor structures for getting transformerless hybrid DC-DC PWM converters," *IEEE Trans. Circuits Syst. I, Reg. Papers*, Vol. 55, No. 2, pp. 687–696, Mar. 2008.
 - [8] O. Abutbul, A. Gherlitz, Y. Berkovich, and A. Ioinovici, "Step-up switching-mode converter with high voltage gain using a switched capacitor circuit," *IEEE Trans. Circuits Syst. I, Fundam. Theory Appl.*, Vol. 50, No. 8, pp. 1098–1102, Aug. 2003.
 - [9] Y. Tang, D. J. Fu, and T. Wang, "Hybrid switched-inductor converters for high step-up conversion," *IEEE Trans. Ind. Electron.*, Vol. 62, No. 3, pp. 1480–1490, Mar. 2015.
 - [10] Y. Jiao, F. L. Luo, and M. Zhu, "Voltage-lift-type switched-inductor cells for enhancing DC-DC boost ability: principles and integrations in Luo converter," *IET Power Electronics*, Vol. 4, No. 1, pp. 131–142, Jan. 2011.
 - [11] F. L. Luo and H. Ye, "Positive output super-lift converters," *IEEE Trans. Power Electron.*, Vol. 18, No. 1, pp. 105–113, 2003.
 - [12] F. L. Luo and H. Ye, "Positive output multiple-lift push-pull switched-capacitor Luo-converters," *IEEE Trans. Ind. Electron.*, Vol. 51, No. 3, pp. 594–602, Jun. 2004.
 - [13] X. Hu and C. Gong, "A high voltage gain DC-DC converter integrating coupled-inductor and diode-capacitor techniques," *IEEE Trans. Power Electron.*, Vol. 29, No. 2, pp. 789–800, Feb. 2014.
 - [14] R. J. Wai and R. Y. Duan, "High-efficiency DC/DC converter with high voltage gain," *IEE Proceedings Electric Power Applications*, Vol. 152, No. 4, pp. 793–802, Jul. 2005.
 - [15] X. Hu and C. Gong, "A high voltage gain DC-DC converter integrating coupled-inductor and diode-capacitor techniques," *IEEE Trans. Power Electron.*, Vol. 29, No. 2, pp. 789–800, Feb. 2014.
 - [16] L. S. Yang, T. J. Liang, and J. F. Chen, "Transformerless DC-DC converters with high step-up voltage gain," *IEEE Trans. Ind. Electron.*, Vol. 56, No. 8, pp. 3144–3152, Aug. 2009.
 - [17] B. R. Lin and F. Y. Hsieh, "Soft-switching zeta-flyback converter with a buck-boost type of active clamp," *IEEE Trans. Ind. Electron.*, Vol. 54, No. 5, pp. 2813–2822, Oct. 2007.
 - [18] T. F. Wu, Y. S. Lai, J. C. Hung, and Y. M. Chen, "Boost converter with coupled inductors and buck-boost type of active clamp," in *IEEE 36th Power Electronics Specialists Conference*, pp. 399–405, Jun. 2005.
 - [19] Y. P. Hsieh, J. F. Chen, T. J. Liang, and L. S. Yang, "Novel high step-Up DC-DC converter for distributed generation system," *IEEE Trans. Ind. Electron.*, Vol. 60, No. 4, pp. 1473–1482, Apr. 2013.
 - [20] Y. P. Hsieh, J. F. Chen, T. J. Liang, and L. S. Yang, "A novel high step-up DC-DC converter for a microgrid system," *IEEE Trans. Power Electron.*, Vol. 26, No. 4, pp. 1127–1136, Apr. 2011.
 - [21] Q. Zhao and F. C. Lee, "High-efficiency, high step-up DC-DC converters," *IEEE Trans. Power Electron.*, Vol. 18, No. 1, pp. 65–73, Jan. 2003.
 - [22] F. Zhang, L. Du, F. Z. Pen, and Z. M. Qian, "A new design method for high-power high-efficiency switched-capacitor DC-DC converters," *IEEE Trans. Power Electron.*, Vol. 23, No. 2, pp. 832–840, Mar. 2008.
 - [23] O. Abutbul, A. Gherlitz, Y. Berkovich, and A. Ioinovici, "Step-up switching-mode converter with high voltage gain using a switched-capacitor circuit," *IEEE Trans. Circuits Syst. I, Fundam. Theory Appl.*, Vol. 50, No. 8, pp. 1098–1102, Aug. 2003.
 - [24] R. J. Wai and R. Y. Duan, "High step-up converter with coupled-inductor," *IEEE Trans. Power Electron.*, Vol. 20, No. 5, pp. 1025–1035, Sep. 2005.
 - [25] Q. Zhao and F. C. Lee, "High performance coupled-inductor DC-DC converters," in *18th Annual IEEE Applied Power Electronics Conference and Exposition(APEC)*, Vol. 1, pp. 109–113, Feb. 2003.
 - [26] R. J. Wai, L. W. Liu, and R. Y. Duan, "High-efficiency voltage-clamped DC-DC converter with reduced reverse-recovery current and switch voltage stress," *IEEE Trans. Ind. Electron.*, Vol. 53, No. 1, pp. 272–280, Feb. 2006.
 - [27] Q. M. Luo, Y. Zhang, P. J. Sun, and L. W. Zhou, "An active clamp high step-up boost converter with a coupled inductor," *Journal of Power Electronics*, Vol. 15, No. 1, pp. 86–95, Jan. 2015.
 - [28] S. K. Changchien, T. J. Liang, J. F. Chen, and L. S. Yang, "Step-up DC-DC converter by coupled inductor and voltage-lift technique," *IET Power Electronics*, Vol. 3, No. 3, pp. 369–378, May 2010.
 - [29] Y. Tang, D. J. Fu, T. Wang, and Z. W. Xu, "Analysis of active-network converter with coupled inductors," *IEEE Trans. Power Electron.*, Vol. 30, No. 9, pp. 4874–4882, Sep. 2015.
 - [30] Y. Zhao, W. H. Li, and X. N. He, "Single-phase improved active clamp coupled-inductor-based converter with extended voltage doubler cell," *IEEE Trans. Power Electron.*, Vol. 27, No. 6, pp. 2869–2878, Jun. 2012.



Hongchen Liu received his B.S. degree in Electrical Engineering from the Northeast Agricultural University, Harbin, China, in 2001; and his M.S. and Ph.D. degrees in Electrical Engineering from the Harbin Institute of Technology (HIT), Harbin, China, in 2003 and 2007, respectively. In 2009, he joined the Department of Electrical Engineering, HIT, as a Lecturer, where he has been an Associate Professor of Electrical Engineering since 2012. From 2008 to 2012, he was a Postdoctoral Fellow of Measuring and Controlling Technology and Instrument. He has authored more than 30 technical papers published in journals and conference proceedings. His current research interests include DC/DC converters and inverters in photovoltaic systems, Matrix converters, and nonlinear dynamics in power electronics.



Jian Ai received his B.S. degree in Electrical Engineering and Automatic from the Heilongjiang University of Science and Technology (USTH), Harbin, China, in 2012. He is presently working towards his M.S. degree in Power Electronics and Electrical Drives in the School of Electrical and Control Engineering, USTH. His current research interests include DC/DC topologies and control in power electronics.



Fei Li received his B.S. degree in Electrical Engineering from HeiLongjiang University, Harbin, China, in 2011, and his M.S. degree in Electrical Engineering from the Harbin Institute of Technology(HIT), Harbin, China, in 2013. He is presently working toward his Ph.D. degree in Power Electronics and Electrical Drives in the School of Electrical Engineering and Automation, HIT. His current research interests include DC/DC topologies, control and nonlinear dynamics in power electronics.